Growth and fabrication of GaN/Er:GaN/GaN core-cladding planar waveguides (EP)

View Online　　Export Citation　　CrossMark

Z. Y. Sun, Y. Q. Yan, (iD) T. B. Smith, W. P. Zhao, J. Li, (iD) J. Y. Lin, (iD) and H. X. Jiang[a] (iD)

AFFILIATIONS

Department of Electrical and Computer Engineering, Texas Tech University, Lubbock, Texas 79409, USA

[a] hx.jiang@ttu.edu

ABSTRACT

Erbium doped gallium nitride (Er:GaN) bulk crystals have emerged as a promising optical gain material for high energy lasers (HELs) operating at the 1.5 μm "retina-safe" spectral region. Among the many designs of HEL gain medium, the core-cladding planar waveguide (PWG) structure is highly desired due to its abilities to provide excellent optical confinement and heat dissipation. We report the realization of a GaN/Er:GaN/GaN core-cladding PWG structure synthesized by hydride vapor phase epitaxy and processed by mechanical and chemical-mechanical polishing. An Er doping concentration of [Er] $= 3 \times 10^{19}$ atoms/cm^3 has been attained in the core layer, as confirmed by secondary ion mass spectrometry measurements. A strong 1.54 μm emission line was detected from the structure under 980 nm resonant excitation. It was shown that these PWGs can achieve a 96% optical confinement in the Er:GaN core layer having a thickness of 50 μm and [Er] $= 3 \times 10^{19}$ atoms/cm^3. This work represents an important step toward the realization of practical Er:GaN gain medium for retina-safe HEL applications.

Solid-state high energy lasers (HELs) have been extensively researched and developed over the last several decades for a vast number of applications in industrial processing, communications, defense, spectroscopy, imaging, and medicine.[1] The optical gain medium is the key which determines the performance of a HEL system. Presently, neodymium doped YAG (Nd:YAG) emitting at 1.06 μm is one of the dominant gain media for HELs due partly to the highly developed crystal growth technologies of Nd:YAG. However, the 1.5 μm wavelength window is retina-safe as this wavelength is absorbed by the surface of the eye instead of being focused inside at the retina[2,3] as well as with a better atmospheric transmittance than that of 1.06 μm.[4] Progress has been made in developing HELs based on Er doped YAG (Er:YAG) operating near 1.5 μm.[5–11] However, the relatively poor thermal properties of the host material YAG, including its relatively low thermal conductivity of $\kappa = 14$ W/(m K) and high thermal expansion coefficient of $\alpha \approx 8 \times 10^{-6}$°C^{-1}, limit further improvement in the operating power of HELs based on the YAG host material.
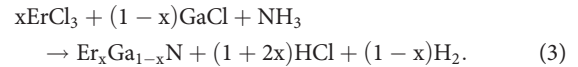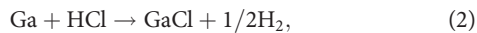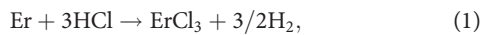
Er doped GaN (Er:GaN) bulk crystals possess vast potential as a gain medium for HELs. First, GaN has a much higher thermal conductivity $\kappa = 253$ W/(m K) and smaller thermal expansion coefficient $\alpha \approx 3.53 \times 10^{-6}$°C^{-1} than YAG.[12] The thermal shock parameter of a typical solid-state laser gain medium attached to a heat sink, κ/α^2, indicates that the maximal attainable laser power for a GaN based laser

is potentially 2 orders of magnitude higher than that for a YAG based laser.[13,14] Moreover, with GaN possessing a small variation of the refractive index (n) with temperature (T), $dn/dT = 0.7 \times 10^{-5}$°C^{-1} at 1.5 μm,[15] GaN potentially provides an excellent beam quality. Furthermore, it was shown that the 1.5 μm emission in Er:GaN has an excellent thermal stability because GaN has a wide energy bandgap.[16–18]

Compared with gain media in the bulk geometries such as disks, rods, and slabs, core-cladding planar waveguides (PWGs) have the advantages of enhanced optical gain and reduced lasing threshold as the optical energy is confined in the core layer (waveguide). Meanwhile, core-cladding PWGs possess sufficiently large surface areas to provide an excellent heat removal capability, thereby minimizing the thermal impact during high power operation. The core-cladding PWGs are also highly compatible with high-power laser diode pumping schemes.[19] Therefore, GaN/Er:GaN/GaN core-cladding PWG represents a very promising design architecture to realize practical applications of Er:GaN crystals as a gain medium for HELs and laser illuminators. Most of the previously studied GaN waveguide structures were based on undoped or unintentionally doped GaN thin epilayers of a few microns in thickness for passive integrated photonic device applications.[20–22] Waveguide structures incorporating ~0.5 μm thick Er:GaN were fabricated on sapphire substrates for studying the basic optical properties, including the carrier

lifetime,[23] excitation and absorption cross sections,[24,25] and optical loss.[26] Waveguide based Er doped GaN and InGaN thin epilayers were fabricated to demonstrate the optical amplification effect under band-edge excitation targeting for applications in chip-scale optical communications.[27] However, core-cladding waveguide structures based on quasibulk crystals of thick Er:GaN and undoped GaN layers for HEL applications have not been explored.

In this work, we report the realization of core-cladding PWGs based on the quasibulk GaN/Er:GaN material system. The hydride vapor phase epitaxy (HVPE) technique was utilized to synthesize the structure, owing to its abilities to employ high purity precursors to provide quasibulk GaN growth with high crystalline quality at a growth rate as high as 100 s of micrometers per hour.[28] To accommodate the incorporation of Er, our HVPE growth system was specially designed in such a way that Ga and Er metal sources are held in separate boats. During HVPE growth, in the metal source zone of the reactor, the metal chlorides of GaCl and ErCl$_3$ are generated from the reactions between the hydrogen chloride (HCl) gas and the metal sources with Ga and Er metal sources being held in different source boats. With this configuration, Ga and Er can be individually controlled so that both undoped GaN and Er:GaN with different Er doping levels can be grown by controlling the growth parameters, including the flow rates of HCl gas passing through each metal source. The metal chlorides were transported by the H$_2$ carrier gas to the growth zone of the reactor, where ammonia (NH$_3$) and metal chlorides reacted to produce Er:GaN on the substrate. During the growth of Er:GaN, the reactor was kept under reduced pressure, whereas the metal source zone of the reactor was heated to 800 °C–1000 °C and the growth zone of the reactor was heated to 1000 °C–1100 °C. The chemical reactions can be described by the following equations:

$$Er + 3HCl \rightarrow ErCl_3 + 3/2H_2, \quad (1)$$

$$Ga + HCl \rightarrow GaCl + 1/2H_2, \quad (2)$$

$$xErCl_3 + (1-x)GaCl + NH_3$$
$$\rightarrow Er_xGa_{1-x}N + (1+2x)HCl + (1-x)H_2. \quad (3)$$

With x = 0, the equations reduce to the growth for undoped GaN.

As illustrated in Figs. 1(a)–1(g), starting from an epi-ready undoped GaN bulk substrate, a 20 μm transition layer with the Er doping level gradually increasing from undoped GaN to Er:GaN was grown, followed by a ~100 μm Er:GaN layer growth with a uniform Er doping concentration. The grown Er:GaN/GaN sample was taken out from the HVPE reactor and processed by lapping and mechanical and chemical-mechanical polishing (CMP) to attain a desired thickness (e.g., with a 30 μm thick Er:GaN core layer) as well as an epi-ready state for the surface of the Er:GaN core layer. The polished sample was put back into the HVPE reactor for the growth of another 20 μm transition layer with the Er doping level gradually decreasing from Er:GaN to undoped GaN, followed by the growth of ~400 μm thick undoped GaN as the top cladding layer. After the HVPE growth, the top cladding surface was polished, and the sample was cut into desired sizes and each facet was polished to obtain the core-cladding PWGs. Figure 1(h) shows an SEM image of the cross section (sidewall) of a processed PWG. The interface between the GaN substrate and the Er:GaN core was well-defined, whereas the interface between the core and the top GaN cladding was less clear. To minimize the scattering loss at the interfaces between the core and the claddings, the rms roughness of the top Er:GaN core layer was controlled by CMP to below 2 nm, as shown in the atomic force microscopy (AFM) image in the inset (a1) of Fig. 2.

To confirm the Er doping level at the Er:GaN core layer of a GaN/Er:GaN/GaN core-cladding PWG, secondary ion mass spectrometry (SIMS) measurements were conducted on the Er:GaN core layer by polishing the layer down to a certain thickness [corresponding to the structure of Fig. 1(c)]. An average Er doping concentration of 3×10^{19} atoms/cm^3 was confirmed and shown in the inset (a2) of Fig. 2(a). Optical images of the core-cladding PWG in 3 processing
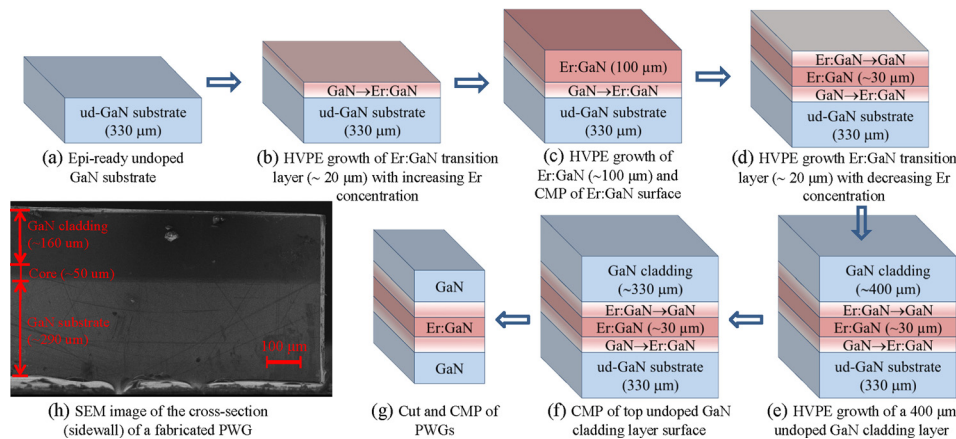

FIG. 1. (a)–(g) Processing flow-chart for obtaining GaN/Er:GaN/GaN core-cladding planar waveguides (PWGs). (a) Starting with c-plane undoped GaN substrates. (b) HVPE growth of a transition layer with Er doping increasing gradually. (c) HVPE growth of the Er:GaN active core layer followed by thinning and epi-polishing of the Er:GaN active core layer. (d) HVPE growth of a transition layer with Er doping decreasing gradually. (e) HVPE growth of the top undoped GaN cladding layer. (f) Polishing of the top cladding layer. (g) Cutting and polishing into core-cladding PWGs. (h) SEM image of the cross section (sidewall) of a fabricated GaN/Er:GaN/GaN PWG, in which the Er:GaN core layer also includes the transition layers as described in (b) and (d).
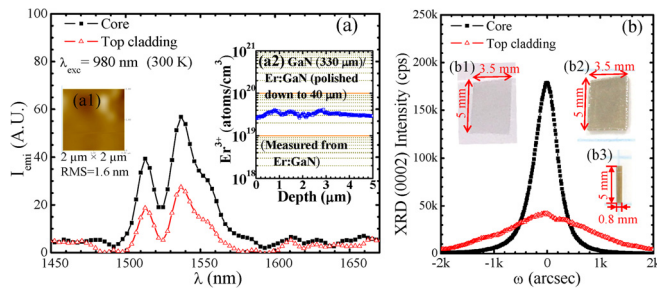
FIG. 2. (a) Room temperature PL spectra ($\lambda_{exc} = 980$ nm) and (b) XRD rocking curves of the GaN (0002) diffraction peak, measured from a core-cladding PWG. Solid black squares are data obtained from the core Er:GaN layer (40 μm) prior to the growth of the top GaN cladding layer for the structure of GaN (330 μm)/Er:GaN (40 μm). Open red triangles are data obtained from the top GaN cladding layer for the structure of GaN (330 μm)/Er:GaN (40 μm)/GaN (300 μm). The inset (a1) of (a) shows an atomic force microscopy (AFM) image, with a scan area of 2 μm × 2 μm and an rms roughness of 1.6 nm, taken at the polished surface of the Er:GaN core layer before the growth of the transition layer and top GaN cladding layer. The inset (a2) of (a) shows the Er concentration profile in the Er:GaN core layer probed by SIMS for a PWG consisting of GaN (330 μm)/Er:GaN (40 μm). The insets of (b) show images of (b1) GaN (330 μm)/Er:GaN (40 μm) prior to the HVPE growth of the top GaN cladding layer; (b2) GaN (330 μm)/Er:GaN (40 μm)/GaN (300 μm) PWG, after HVPE growth of the top GaN cladding layer; (b3) a fabricated GaN/Er:GaN/GaN core-cladding PWG.

stages are shown in the insets of Fig. 2(b). The inset (b1) of Fig. 2(b) shows the image of a polished Er:GaN core layer surface prior to the HVPE growth of the top GaN cladding layer, with a structure of GaN (330 μm)/Er:GaN (40 μm). The inset (b2) of Fig. 2(b) shows the image of the top as-grown surface of the same sample after HVPE growth of the top GaN cladding layer, with a completed structure of GaN (330 μm)/Er:GaN (40 μm)/GaN (300 μm). The inset (b3) of Fig. 2(b) shows an example of a core-cladding PWG fabricated from the core-cladding GaN/Er:GaN/GaN sample.

Photoluminescence (PL) emission characteristics at the 1.5 μm window of interest have been studied under 980 nm excitation, which resonantly excites carriers from the $^4I_{15/2}$ ground state to the $^4I_{11/2}$ second excited state manifolds of Er^{3+} ions with an excitation cross section of about 2.2×10^{-21} cm^2 (Refs. 15 and 16) and an optical penetration depth of >1 mm. A strong 1.5 μm emission line originating from the radiative transition from the first excited to the ground state ($^4I_{13/2} \rightarrow {}^4I_{15/2}$) of Er^{3+} ions was observed from the Er:GaN core layer within a GaN/Er:GaN/GaN core-cladding PWG. As illustrated in Fig. 2(a), the higher intensity spectrum (solid black square result) was measured from the Er:GaN core layer prior to the growth of the top GaN cladding layer, while the lower intensity spectrum (open red triangles) was measured from the top GaN cladding layer after completing the HVPE growth of the core-cladding structure. For the latter case, both the excitation photons at 980 nm and PL emission photons at 1.5 μm had to penetrate through the top GaN cladding layer, resulting in a lower measured PL intensity than that measured directly at the top of the Er:GaN core layer (solid black squares). This reduction in the measured PL intensity is partly caused by the optical loss due to scattering by the relatively rough as-grown surface of the top GaN cladding layer. To validate this speculation, the relative crystalline qualities of these structures were probed and compared. The results for X-ray diffraction (XRD) rocking curves of the GaN (0002) diffraction peak are shown in Fig. 2(b). Before the growth of

the top GaN cladding layer, the Er:GaN (40 μm) core layer has an XRD rocking of the (0002) peak linewidth (FWHM) of 515 arc sec (solid black squares). However, after the growth of the core-cladding PWG structure was completed, the XRD rocking of the (0002) peak of the top GaN cladding layer exhibits a much broader FWHM of 1937 arc sec and lower XRD peak intensity. The deterioration of the crystalline quality for the top GaN cladding layer is possibly due to a slight lattice mismatch between Er:GaN and GaN layers, which results in the accumulation of strain as the undoped GaN cladding layer gets thicker. The results thus suggest that optimization of the transition layers between Er:GaN and undoped GaN cladding layers is still necessary to further improve the overall material quality of the GaN/Er:GaN/GaN core-cladding PWGs.

Figure 3 shows the optical intensity distribution in a GaN (200 μm)/Er:GaN (50 μm)/GaN (200 μm) core-cladding PWG structure shown in Fig. 3(a) with a waveguide width of 1 mm in the horizontal (x−) direction and a length of 5 mm in the propagation (z−) direction. With the Er doping concentration of (Er) = 3×10^{19} atoms/cm^3 in the core layer, the refractive index difference between the Er:GaN core layer and the GaN cladding layer will be 0.00172.[29] Figure 3(b) shows the simulated optical intensity distribution across the core Er:GaN (50 μm) and along the propagation z-direction. Figure 3(c) shows the transverse mode profile of the x-y cross section at any z position, indicating a good optical confinement. Figure 3(d) shows the corresponding mode amplitude profile along the y-axis (across the Er:GaN core region) at any z position. A 96% of optical confinement of the power can be achieved at the 50 μm Er:GaN core region. By increasing the thickness or the doping concentration of the Er:GaN core layer, the optical confinement factor (%) can be further increased. The results are thus indicative of a potentially good efficiency for the pumping laser that excites the Er^{3+} ions in the GaN/Er:GaN/GaN core-cladding PWGs.
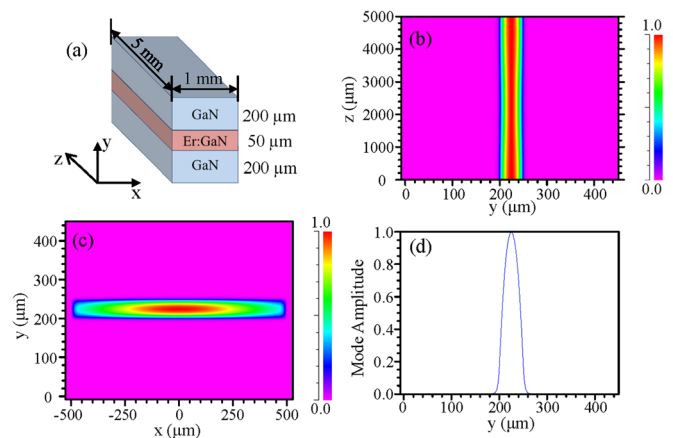

FIG. 3. Simulated optical intensity distribution of a GaN/Er:GaN/GaN core-cladding PWG. (a) Schematic of a GaN/Er:GaN/GaN core-cladding PWG, with a 50 μm Er:GaN core and 200 μm GaN claddings. The waveguide structure has a width (along x-axis) of 1 mm and a length (along z-axis) of 5 mm and an Er doping concentration in the core of 3×10^{19} atoms/cm^3. (b) Optical intensity distribution across the Er:GaN core region and along the propagation direction, z-axis. (c) Transverse mode profile of the x-y cross sectional plane. (d) Mode amplitude profile along the y-axis.
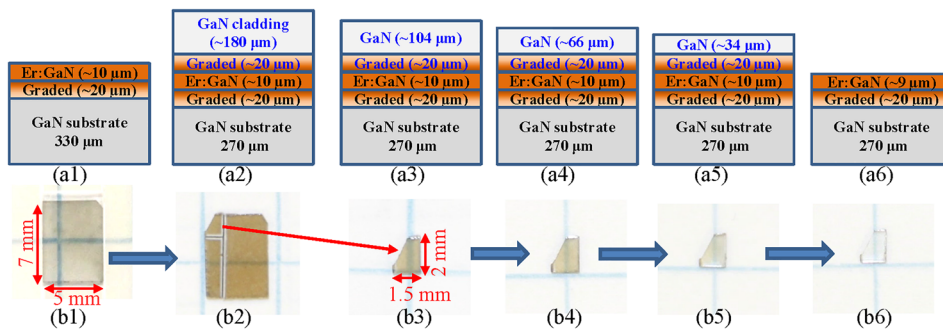
FIG. 4. Schematics of the layer structures (a1)–(a6) and the corresponding optical images (b1)–(b6) illustrating the thinning of a GaN/Er:GaN/GaN core-cladding structure by polishing. Before (b1) and after (b2) growth of the top GaN cladding layer. Reducing the top GaN cladding layer by mechanical polishing (b3)–(b6).

The origin of the yellowish color exhibited by the top GaN cladding layer [shown in the inset (b2) of Fig. 2(b)] was also investigated. Figures 4(a1)–4(a6) show the various stages of a GaN/Er:GaN/GaN core-cladding structure prepared for analysis by polishing down from the top cladding layer and Figs. 4(b1)–4(b6) show the corresponding images of the same evolving GaN/Er:GaN/GaN core-cladding structure. Figure 4(b1) shows that the Er:GaN core layer with a total thickness of $\sim 30\,\mu m$ prior to the growth of the top cladding layer exhibits almost no yellowish color. After the growth of the top GaN cladding layer, the sample became visibly yellowish, as revealed in Fig. 4(b2). Figures 4(b3)–4(b5) illustrate that as the top GaN cladding layer was polished to reduced thicknesses, the yellowish color was also diminishing. Figure 4(b6) reveals that the yellowish color completely disappeared when the top GaN cladding layer was fully removed. When the top GaN cladding layer was polished down to $104\,\mu m$, corresponding to the structure shown in Fig. 4(a3), PL emission excited by 193 nm photons was measured from the top cladding layer and a room temperature PL spectrum is shown in Fig. 5. Since the optical penetration depth of the above bandgap photons in GaN is about $1\,\mu m$, the PL excited by 193 nm is considered to result solely from the top GaN cladding layer. The top cladding layer exhibits a strong band edge transition at 3.4 eV and another considerably broader emission line around 2.5 eV. The emission line near 2.5 eV is well known as "the yellow line" in GaN related to the presence of native defects in GaN.[30–32] Based on
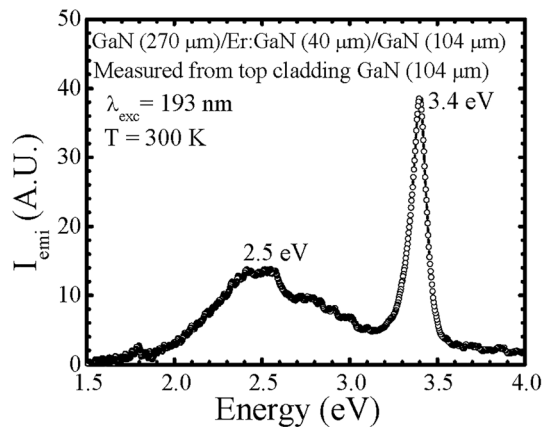
previous studies,[30–32] we suggest that the origin of the yellow line in the GaN cladding layer is related to a defect center, most likely involving gallium vacancy complexes $(V_{Ga}\text{-}O_N)^{2-/1-}$. Strain accumulation with the increasing layer thickness due to lattice mismatch between Er:GaN and GaN seems to enhance the generation of $(V_{Ga}\text{-}O_N)$ complexes in the top GaN cladding layer.

In summary, GaN/Er:GaN/GaN core-cladding PWGs have been produced by HVPE growth. An average Er doping concentration of 3×10^{19} atoms/cm^3 in the core region has been attained as confirmed by SIMS analysis. The structure exhibits a strong $1.5\,\mu m$ Er^{3+} PL emission under 980 nm resonant excitation and good crystalline quality of the Er:GaN core layer. Simulation results indicated a good optical confinement in the Er:GaN core. The physical origin of the yellowish color of the top GaN cladding layer was investigated and attributed to the presence of Ga vacancy complexes. The realization of GaN/Er:GaN/GaN core-cladding PWGs marks a significant step toward practical implementation of Er:GaN as a promising gain material for retina-safe optical amplifiers or HELs. The layer structure of GaN/Er:GaN/GaN core-cladding PWGs can be further optimized in terms of the thickness and Er doping concentration of the Er:GaN core and length of the waveguides. The optical pumping configuration can also be optimized to achieve improved optical pumping efficiency. Moreover, further optimization of the transition layer between Er:GaN and undoped GaN cladding layers is expected to mitigate to a certain degree the issue of yellowish color in the top GaN cladding layer. With further development, it is anticipated that GaN/Er:GaN/GaN core-cladding PWGs demonstrated here can be adopted by industries to develop next generation HEL systems with improved thermal-mechanical properties, eye-safety, and maximum optical power delivery capability.

FIG. 5. (a) Room temperature PL spectrum ($\lambda_{exc} = 193\,nm$) measured from the top GaN cladding layer, for a core-cladding structure of GaN (270 μm)/Er:GaN (40 μm)/GaN (104 μm).

REFERENCES

[1]Y. Kalisky and O. Kalisky, Opt. Eng. **49**, 091003 (2010).
[2]E. A. Boettner and J. R. Wolter, Invest. Ophthalmol. Visual Sci. **1**, 776 (1962).
[3]J. A. Zuclich, D. J. Lund, and B. E. Stuck, Health Phys. **92**, 15 (2007).
[4]J. Bailey, A. Simpson, and D. Crisp, Publ. Astron. Soc. Pac. **119**, 228 (2007).
[5]Y. X. Fan and R. G. Schlecht, U.S. patent 4,995,046 (Feb. 19, 1991).

[6]N. Ter-Gabrielyan, V. Fromzel, X. Mu, H. Meissner, and M. Dubinskii, Opt. Lett. **38**, 2431 (2013).

[7]K. Spariosu, V. Leyva, R. A. Reeder, and M. J. Klotz, IEEE J. Quantum Electron. **42**, 182 (2006).

[8]J. O. White, IEEE J. Quantum Electron. **45**, 1213 (2009).

[9]M. Němec, J. Šulc, L. Indra, M. Fibrich, and H. Jelínková, Laser Phys. **25**, 015803 (2015).

[10]T. Sanamyan, J. Opt. Soc. Am. B **33**, D1 (2016).

[11]D. J. Ottaway, L. Harris, and P. J. Veitch, Opt. Express **24**, 15341 (2016).

[12]H. Shibata, Y. Waseda, H. Ohta, K. Kiyomi, K. Shimoyama, K. Fujito, H. Nagaoka, Y. Kagamitani, R. Simura, and T. Fukuda, Mater. Trans. **48**, 2782 (2007).

[13]D. C. Brown, IEEE J. Quantum Electron. **33**, 861 (1997).

[14]T. Taira, C. R. Phys. **8**, 138 (2007).

[15]R. Hui, Y. Wan, J. Li, S. X. Jin, J. Y. Lin, and H. X. Jiang, IEEE J. Quantum Electron. **41**, 100 (2005).

[16]P. N. Favennec, H. L'Haridon, M. Salvi, D. Moutonnet, and Y. Le Guillou, Electron. Lett. **25**, 718 (1989).

[17]C. Ugolini, N. Nepal, J. Y. Lin, and H. X. Jiang, Appl. Phys. Lett. **89**, 151903 (2006).

[18]Z. Y. Sun, J. Li, W. P. Zhao, J. Y. Lin, and H. X. Jiang, Appl. Phys. Lett. **109**, 052101 (2016).

[19]C. Grivas, Prog. Quantum Electron. **35**, 159 (2011).

[20]H. Chen, H. Fu, X. Huang, X. Zhang, T.-H. Yang, J. A. Montes, I. Baranowski, and Y. Zhao, Opt. Express **25**, 31758 (2017).

[21]T. Sekiya, T. Sasaki, and K. Hane, J. Vac. Sci. Technol. **33**, 031207 (2015).

[22]O. Westreich, G. Atar, Y. Paltiel, and N. Sicron, Phys. Status Solidi A **215**, 1700551 (2018).

[23]Q. Wang, R. Hui, R. Dahal, J. Y. Lin, and H. X. Jiang, Appl. Phys. Lett. **97**, 241105 (2010).

[24]Q. Wang, R. Dahal, I.-W. Feng, J. Y. Lin, H. X. Jiang, and R. Hui, Appl. Phys. Lett. **99**, 121106 (2011).

[25]R. Hui, R. Xie, I. W. Feng, Z. Y. Sun, J. Y. Lin, and H. X. Jiang, Appl. Phys. Lett. **105**, 051106 (2014).

[26]I. W. Feng, W. P. Zhao, J. Li, J. Y. Lin, H. X. Jiang, and J. Zavada, Appl. Opt. **52**, 5426 (2013).

[27]R. Dahal, C. Ugolini, J. Y. Lin, H. X. Jiang, and J. M. Zavada, Appl. Phys. Lett. **95**, 111109 (2009).

[28]K. Motoki, T. Okahisa, S. Nakahata, N. Matsumoto, H. Kimura, H. Kasai, K. Takemoto, K. Uematsu, M. Ueno, Y. Kumagai, A. Koukitu, and H. Seki, J. Cryst. Growth **237–239**, Part 2, 912 (2002).

[29]S. Alajlouni, Z. Y. Sun, J. Li, J. M. Zavada, J. Y. Lin, and H. X. Jiang, Appl. Phys. Lett. **105**, 081104 (2014).

[30]T. Mattila and R. M. Nieminen, Phys. Rev. B **55**, 9571 (1997).

[31]S. Limpijumnong and C. G. Van de Walle, Phys. Rev. B **69**, 035207 (2004).

[32]A. Sedhain, J. Li, J. Y. Lin, and H. X. Jiang, Appl. Phys. Lett. **96**, 151902 (2010).